Biochemical Society Transactions (2022) **50** 1081–1090
https://doi.org/10.1042/BST20211131

PORTLAND PRESS

Review Article

CDK activity sensors: genetically encoded ratiometric biosensors for live analysis of the cell cycle

Michael A. Q. Martinez and David Q. Matus

Department of Biochemistry and Cell Biology, Stony Brook University, Stony Brook, NY 11794, U.S.A

Correspondence: David Q. Matus (david.matus@stonybrook.edu)

Cyclin-dependent kinase (CDK) sensors have facilitated investigations of the cell cycle in living cells. These genetically encoded fluorescent biosensors change their subcellular location upon activation of CDKs. Activation is primarily regulated by their association with cyclins, which in turn trigger cell-cycle progression. In the absence of CDK activity, cells exit the cell cycle and become quiescent, a key step in stem cell maintenance and cancer cell dormancy. The evolutionary conservation of CDKs has allowed for the rapid development of CDK activity sensors for cell lines and several research organisms, including nematodes, fish, and flies. CDK activity sensors are utilized for their ability to visualize the exact moment of cell-cycle commitment. This has provided a breakthrough in understanding the proliferation-quiescence decision. Further adoption of these biosensors will usher in new discoveries focused on the cell-cycle regulation of development, ageing, and cancer.

Introduction

The cell cycle was conceptualized nearly 70 years ago by Howard and Pelc [1]. By studying the process of DNA synthesis through a radioactive labeling technique, they established that the cell cycle consists of four phases: G1, S, G2, and M. The first gap phase (G1) occurs prior to DNA synthesis (S), followed by a second gap phase (G2), and finally mitosis (M). During mitosis, nuclear division and cytokinesis occurs, giving rise to two daughter cells. Each phase varies in length, and progression through the cell cycle is largely driven by cyclins and cyclin-dependent kinases (CDKs). The integrity of the cell cycle is maintained by checkpoints. The G1 checkpoint is known as the restriction point [2]. Cells that have crossed the restriction point are committed to completing the cell cycle. Cells that have not crossed the restriction point remain in G1 or enter a quiescent phase called G0. Since the concept of the cell cycle was first introduced, the field has exploded, providing fundamental insights into biological processes such as development, homeostasis, and regeneration. Studies of the cell cycle also impact our understanding of cancer (reviewed in [3]), and many chemotherapies are designed to halt cell-cycle progression.

Techniques such as flow cytometry, immunostaining, and synchronization were commonly used to analyze the cell cycle. While these techniques are still in use today, valuable kinetic information about the cell cycle is lost in individual cells and heterogeneous populations. Advanced genetic approaches have allowed live visualization of the cell cycle through fluorescently tagged proteins, peptides, or degrons. Sakaue-Sawano et al. [4] developed the fluorescent ubiquitination-based cell cycle indicator (FUCCI) system, revolutionizing our analysis of the cell cycle in living cells. The FUCCI system consists of two fluorescent proteins fused to degrons derived from Cdt1 and Geminin. Visualization of the Cdt1 degron is restricted to the G1 and G0 phase of the cell cycle, while the Geminin degron is visualized in S, G2, and M. The E3 ubiquitin ligases SCF^{Skp2} and APC/C^{Cdh1} recognize the Cdt1 and

Received: 18 February 2022
Revised: 9 May 2022
Accepted: 18 May 2022

Version of Record published:
8 June 2022

Biochemical Society Transactions (2022) **50** 1081–1090
https://doi.org/10.1042/BST20211131

Geminin degrons, respectively, and prevent the overlapping accumulation of these degrons in the cell cycle by targeting them for degradation. Thus, the reciprocal expression of each component of the FUCCI system allows visual detection of either G1/G0 or S/G2/M.

From the time the FUCCI system was first developed, there have been numerous advances [5–13] as well as adaptations for a variety of research organisms [14–20]. Still, one of the major drawbacks of the FUCCI system has been the inability to discriminate between cells in G1 and G0 [21]. The ability to visualize G0 has clinical implications. Many stem cells and resistant cancer cells exist in a G0 quiescent state [22]. To solve this issue, Oki et al. [9] combined the FUCCI system with a fluorescently tagged p27 mutant lacking CDK inhibitory activity. The rationale behind this approach is that p27 is degraded in G1 but not in G0. However, there are limitations to this approach. Though levels of p27 drop in G1, degradation is not rapid enough to fully distinguish cycling cells from quiescent cells in real time. Also, their method relies on the FUCCI system to visualize an entire cell cycle, from G0 to M. The use of an additional fluorescent reporter does not appear feasible unless a fourth spectrally separable fluorophore is introduced.

The laboratory of Tobias Meyer developed a live-cell fluorescent biosensor that can faithfully distinguish G1 from G0 (Figure 1A) [23,24]. They first truncated a previously identified C-terminal region of human DNA helicase B ($DHB_{957–1087}$) [25] to a 94 amino acid peptide consisting of amino acids 994 to 1087 ($DHB_{994–1087}$). They then fused $DHB_{994–1087}$ to a fluorescent protein for live-cell imaging in culture and determined that the newly truncated version of DHB was sufficient to confer cell cycle-dependent shuttling between the nucleus and cytoplasm. In contrast with $DHB_{957–1087}$, which harbors seven CDK phosphorylation sites, $DHB_{994–1087}$ contains four sites modified by CDKs. These four sites closely and evenly flank a nuclear localization signal (NLS) and are phosphorylated from G1 to G2. Directly adjacent to the NLS is a nuclear export signal (NES). Hence, CDK activation and consequent phosphorylation triggers the nuclear-to-cytoplasmic translocation of

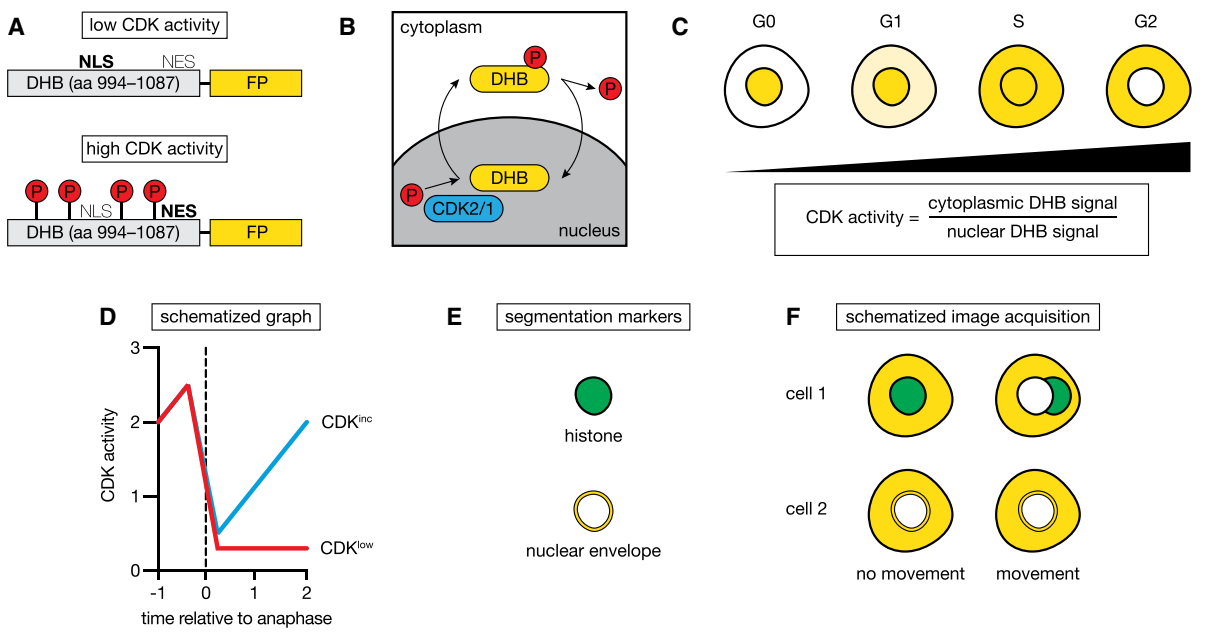

Figure 1. The CDK activity sensor: lights, camera, action.

(**A**) Cartoon of fluorescently tagged CDK activity sensors in the presence of low (top) and high (bottom) CDK activity. (**B**) CDK2 and CDK1 mediate phosphorylation of the CDK activity sensor, leading to its nuclear-to-cytoplasmic translocation. (**C**) Increased cytoplasmic localization represents cell-cycle progression. Equation used to calculate CDK activity is shown. It should be noted that CDK activity is never equal to zero, as noise emanates from the cytoplasm of G0 cells. (**D**) Schematized graph of two single-cell traces illustrating CDK activity in cycling (blue) and quiescent (red) cells. Dashed line indicates the time of anaphase. (**E**) Cartoon of a histone (top) and nuclear envelope (bottom) marker for cell segmentation. (**F**) Schematized image acquisition merging the segmentation markers depicted in (E) with the CDK activity sensor. Labeling the nuclear envelope with the same fluorescent protein as the CDK activity sensor minimizes segmentation to a single channel and avoids issues associated with cell movement during fluorescent channel acquisition.

the sensor by occluding the NLS (Figure 1B). In the absence of CDK activity, the sensor is completely nuclear, which indicates a G0 state. In summary, the CDK activity sensor is a single-color, translocation-based sensor for tracking the cell cycle of individual cells. As the sensor has only recently been introduced in living animals [26–30], we are just beginning to scratch the surface of what the CDK activity sensor can reveal.

CDK activity sensors in cell culture

The CDK activity sensor was previously a G1-phase biosensor [24]. Hahn et al. established several cell lines expressing the G1-phase biosensor, which consists of $DHB_{994–1087}$ fused to the orange fluorescent protein tdimer2(12) (Table 1). $DHB_{994–1087}$-tdimer2(12) was predominantly nuclear in G1 and cytoplasmic in S and G2 until nuclear envelope breakdown. To mark the G1/S and S/G2 transition, Hahn et al. co-expressed a fluorescent S-phase reporter [31]. The main component of this S-phase reporter is proliferating cell nuclear antigen (PCNA), which aggregates at sites of DNA replication. As a proof of principle, the authors used both tools to measure the duration of G1, S, G2, and M in their cell lines of interest. Their analyses revealed a bimodal G1-phase duration in a fibroblast cell line. Furthermore, the authors sought to determine when neuronal differentiation occurs relative to the cell cycle. Features of neuronal differentiation include neurite formation and cell-cycle arrest. Using a neuronal-like cell line expressing the G1-phase biosensor and a fluorescent reporter of the plasma membrane, they induced neuronal differentiation by exposing these cells to neuronal growth factor. Though most cells were arrested in G1, they unexpectedly found neurites emanating from neurons in G1, S, and G2. Together, Hahn et al. demonstrated that the G1-phase biosensor can track the cell cycle of individual cells in culture, revealing subpopulations with different G1 kinetics, and provide a cell-cycle context to cellular processes such as differentiation.

Through a series of biochemical and pharmacological assays, the G1-phase biosensor was validated as a sensor for CDK2 activity by Spencer et al. [23]. These authors modified the G1-phase biosensor by swapping tdimer2(12) for the yellow fluorescent protein mVenus (Table 1). Following this modification, they combined $DHB_{994–1087}$-mVenus with mCerulean-Cdt1 and histone 2B (H2B)-mCherry to track the G1/S and G2/M transition, respectively. Like $DHB_{994–1087}$-tdimer2(12), $DHB_{994–1087}$-mVenus was mostly nuclear in G1 (Figure 1C). However, their subcellular localization patterns were different in S and G2. While $DHB_{994–1087}$-tdimer2(12) was cytoplasmic in S and G2, $DHB_{994–1087}$-mVenus was evenly distributed in the cell in S and nuclear excluded in G2 (Figure 1C). In addition, $DHB_{994–1087}$-mVenus was completely nuclear in G0 (Figure 1C). Because $DHB_{994–1087}$-mVenus senses CDK2 activity and allows for the visual distinction of all interphase states, including G0, the authors used the cytoplasmic-to-nuclear ratio of $DHB_{994–1087}$-mVenus as a cell-cycle indicator and as a quantitative readout for CDK2 activity (Figure 1C). By tracking epithelial and fibroblast cell lines

Table 1 CDK activity sensors in cell culture studies

Transgene	Organism	References
$DHB_{994–1087}$-mTurquoise	Mouse	[34]
$DHB_{994–1087}$-mTurquoise2	Human	[35]
$DHB_{957–1087}$-GFP	Human	[37]
$DHB_{994–1087}$-GFP	Human	[33]
Clover-$DHB_{994–1087}$	Human	[38]
$DHB_{994–1087}$-mVenus	Human, mouse	[23]
$DHB_{994–1087}$-mKO2	Human	[39]
$DHB_{994–1087}$-tdimer2(12)	Human, mouse, rat	[24]
$DHB_{957–1087}$-mRuby	Human	[36]
$DHB_{994–1087}$-mScarlet-I	Chicken	[40]
$DHB_{994–1087}$-mCherry	Human	[41]
mKate2-$DHB_{994–1087}$	Mouse	[43]
$DHB_{994–1087}$-mKate2	Human	[42]
mCherry-$Rb_{886-928}$	Human	[46]

Biochemical Society Transactions (2022) 50 1081–1090
https://doi.org/10.1042/BST20211131

expressing $DHB_{994–1087}$-mVenus, Spencer et al. made a fundamental discovery that transformed our understanding of the cell cycle's restriction point. It was long believed that the proliferation-quiescence decision was made by daughter cells in G1 [2]. However, Spencer et al. demonstrated that the decision is initially made by mother cells in late G2, and a subsequent decision is processed by their daughter cells in G1. Specifically, expression of p21 in the G2-phase of mitotic mother cells drives a bifurcation in CDK2 activity after mitosis, where daughter cells inherit either intermediate or low levels of CDK2 activity (Figure 1D). Only daughter cells with low CDK2 activity retain the decision to proliferate or become quiescent, whereas daughter cells with intermediate CDK2 activity commit to completing the cell cycle. Thus, Spencer et al. expanded the cell-cycle analysis toolkit by adding the CDK2 activity sensor and evoked a larger discussion about the location of the cell cycle's restriction point (reviewed in [32]).

Current literature refers to the $DHB_{994–1087}$ peptide as a CDK activity sensor, as Schwarz et al. [33] demonstrated that $DHB_{994–1087}$ senses both CDK2 and CDK1 activity. CDK activity sensors have been generated in cell lines derived from humans, mice, rats, and chicken (Table 1) [23,24,33–43]. Recently, the CDK activity sensor was visualized in an orthotopic mouse model of human head and neck cancer [44]. The modularity of the CDK activity sensor is reflected in these studies. For example, a wide range of fluorescent proteins have been fused to either the C- or N- terminus of $DHB_{994–1087}$. In addition, the slightly longer version of DHB that consists of amino acids 957 to 1087 ($DHB_{957–1087}$) was shown to behave similarly to $DHB_{994–1087}$ [36,37]. Furthermore, the self-cleaving 2A peptide system has been employed by several groups as it allows for the expression of two or more transgenes under a single promoter. Yoon et al. utilized the 2A system to co-express $DHB_{994–1087}$ and histone H2B [45]. H2B is a nuclear marker during interphase (Figure 1E), allowing for the accurate segmentation of the cytoplasm and nucleus, and a reporter of M-phase upon chromatin condensation. The 2A system was also used by Yang and colleagues to co-express $DHB_{994–1087}$ and a novel reporter of CDK4/6 activation [46]. This reporter is based on a short C-terminal fragment of amino acids 886 to 928 of retinoblastoma (Rb) protein (Table 1). The mechanism and quantification of $Rb_{886–928}$ translocation is similar to that of DHB (Figure 1A–C), though its design is based on the kinase translocation reporter (KTR) strategy developed by the laboratory of Markus Covert [47]. Pairing these biosensors allowed Yang et al. to determine when cycling cells activate CDK4/6 relative to CDK2 by measuring the cytoplasmic-to-nuclear ratios of Rb and DHB, respectively. Taken together, the CDK activity sensor is highly adaptable, and therefore it can be implemented in cell culture studies that explore a breadth of biological phenomena associated with the cell cycle.

CDK activity sensors in nematodes

The laboratory of Sander van den Heuvel published the first CDK activity sensor for *C. elegans* [26]. *C. elegans* is an ideal research organism for studies of the cell cycle because its cell lineage is highly invariant and can be traced at single-cell resolution. Their team began by generating worms expressing $DHB_{994–1087}$-GFP under the control of the ubiquitous *eft-3* promoter (Table 2) [26]. However, expression of $DHB_{994–1087}$-GFP was too strong to distinguish cycling cells from quiescent cells in the soma (but not in the embryo [48]). Next, they drove the expression of $DHB_{994–1087}$-GFP using the *mcm-4* promoter (Table 2). As expected for an E2F target gene promoter, the *mcm-4* promoter was active in proliferating cells, such as seam cells, Q neuroblast cells, and vulval precursor cells. Deng et al. [49] placed $DHB_{994–1087}$-GFP under the control of the anchor cell-specific promoter $lin\text{-}3^{ACEL}$ (Table 2), providing further evidence that the anchor cell of the somatic gonad is arrested in the cell cycle [50], likely in the G0-phase [51]. Therefore, the CDK activity sensor can be used in *C. elegans* to study embryonic and post-embryonic lineages that are cycling or quiescent.

Our laboratory developed an all-encompassing CDK activity sensor for *C. elegans* [27]. Using the 2A system in *C. elegans* [52], we created transgenic lines co-expressing $DHB_{994–1087}$-2xmKate2 and H2B-GFP as well as $DHB_{994–1087}$-GFP and H2B-2xmKate2 under the control of the ubiquitously active ribosomal *rps-27* promoter (Table 2). Unlike the *mcm-4* promoter, *rps-27* drove the expression of $DHB_{994–1087}$ in proliferating cells and cells that have exited the cell cycle. In addition, *rps-27*-driven $DHB_{994–1087}$ was discernable in the embryo, germline, ventral uterine cells, sex myoblasts, and vulval precursor cells. To visually inspect S-phase in somatic cells, we constructed PCN-1-GFP, a C-terminal translational fusion of the *C. elegans* ortholog of PCNA to GFP. Similar to studies performed in cell culture [24] and the *C. elegans* embryo [53], PCN-1-GFP formed subnuclear foci at sites of DNA replication in several post-embryonic lineages (but not in the germline [54]). Co-visualizing the CDK activity sensor and PCNA allowed us to ascertain $DHB_{994–1087}$ ratios for each interphase state. We also generated a line only expressing $DHB_{994–1087}$-2xmKate2 through *rps-27* (Table 2), enabling

Table 2 CDK activity sensors in nematodes, fish, and flies

Organism	Promoter	Transgene	Description	References
C. elegans	*eft-3*	$DHB_{994–1087}$-GFP	Ubiquitously expressed during all stages of development; however, too bright to detect cycling cells in the soma	[26,48]
	mcm-4	$DHB_{994–1087}$-GFP	Expressed in proliferating cells	[26]
	rps-27	$DHB_{994–1087}$-GFP	Ubiquitously expressed during all stages of development	[27]
	rps-27	$DHB_{994–1087}$-2xmKate2	Ubiquitously expressed during all stages of development	[27]
	rps-0	$DHB_{994–1087}$-mKate2	Ubiquitously expressed during all stages of development	[27]
	lin-3^{ACEL}	$DHB_{994–1087}$-GFP	Expressed in the anchor cell	[49]
	unc-62	$DHB_{994–1087}$-2xmKate2	Expressed in the vulval and sex myoblast lineages	[51]
Zebrafish	*hsp70l*	$DHB_{994–1087}$-mNeonGreen	Expressed in the embryo	[27]
	hsp70l	$DHB_{994–1087}$-mScarlet	Expressed in the embryo	[27]
Drosophila	*tubulin*	$DHB_{994–1087}$-mCherry	Expressed in the embryo	[28]

the use of the blue/cyan and green/yellow fluorescent channels. In a variant of this strain, we fused $DHB_{994–1087}$ to one copy of mKate2 under the control of the *rps-0* promoter (Table 2). We recently made a tissue-restrictive $DHB_{994–1087}$-2xmKate2 strain that places the CDK activity sensor in sex myoblasts and vulval precursor cells (Table 2) [51]. In examining several post-embryonic lineages in the worm with the CDK activity sensor, we demonstrated that low levels of CDK activity after mitosis is predictive of cell-cycle exit (Figure 1D) and that CKI-1 (p21/p27) accumulation peaks in mother cells that give rise to post-mitotic daughter cells. Additionally, we revealed a stochastic cell division shortly after mitotic exit in the invariant vulval lineage. This cryptic stochasticity had only been observed at low frequency using end-point lineage analysis [55]. The CDK activity sensor is a valuable addition to the lineage-tracing toolkit for *C. elegans*, and it can be combined with other fluorescently labeled proteins including but not limited to components of the cell cycle [49,51,56].

CDK activity sensors in fish

Together with Benjamin Martin's laboratory, we generated transgenic zebrafish embryos expressing the CDK activity sensor under the control of the heat shock-inducible *hsp70l* promoter [27]. These lines were designed to either co-express $DHB_{994–1087}$-mNeonGreen and H2B-mScarlet or $DHB_{994–1087}$-mScarlet and H2B-miRFP670 (Table 2). To express DHB and H2B, we utilized the 2A system for zebrafish embryos [57]. We also visualized S-phase in $DHB_{994–1087}$-mScarlet embryos by expressing PCNA-GFP (described in [58,59]). This allowed us to infer that the CDK activity sensor was re-locating in a cell cycle-dependent fashion in the tailbud of zebrafish embryos, enabling us to distinguish cycling cells from quiescent cells in several embryonic tissues of interest (Figure 1D). Also, we identified fast- and slow- cycling cells in the tailbud, with the latter appearing to be in a prolonged G1-phase. In sum, we described the first version of the CDK activity sensor for zebrafish, providing a new tool for studying the cell cycle during vertebrate development.

CDK activity sensors in flies

The laboratory of Stefano Di Talia generated the first CDK activity sensor for *Drosophila* [28]. Their team fused $DHB_{994–1087}$ with mCherry on its C-terminus and drove the expression of the CDK activity sensor in embryos (Table 2). During the maternally driven syncytial blastoderm cycles, the CDK activity sensor translocated from the nucleus to the cytoplasm in an oscillating fashion. They were able to prevent the cytoplasmic localization of the CDK activity sensor by mutating the four CDK phosphorylation sites on $DHB_{994–1087}$. The same mutant was generated in mammalian cells [60]. Ultimately, they designed the biosensor to examine the relationship between histone locus body (HLB) growth and CDK activity. HLBs are nuclear bodies that are evolutionarily conserved and responsible for histone biogenesis [61]. After depleting the maternal input of CDK2,

Biochemical Society Transactions (2022) **50** 1081–1090
https://doi.org/10.1042/BST20211131

they were able to conclude that CDKs influence the size of HLBs. Interestingly, the phosphorylation of the CDK activity sensor was unaffected by the loss of CDK2. As CDK1 was shown to contribute to the phosphorylation of the CDK activity sensor in *C. elegans* [26], these data support the idea that the phosphorylation of $DHB_{994–1087}$ by CDK2 and CDK1 is conserved across species (Figure 1B). Overall, this is surprising given that DHB has no known orthologs in invertebrates [62,63].

Experimental considerations

The color palette of CDK activity sensors will continue to expand as new fluorescent proteins are developed and more fluorescent proteins are tested. When choosing a fluorophore, one must consider the protein's brightness, photostability, and monomeric quality [64,65]. No fluorescent protein is perfect for every experimental situation [64]. For example, although GFP is brighter [66], we have noticed an improvement in the CDK activity sensor's dynamic range when using mKate2. The oligomeric tendencies of mKate2 [67] may provide an explanation for the enhanced presence of $DHB_{994–1087}$-mKate2 in the nucleus of G0 cells and the cytoplasm of G2 cells. We speculate that mKate2 oligomerization limits passive diffusion through the nucleus. Yang et al. reported a similar observation when fusing mCherry to the CDK4/6 activation reporter [46]. Thus, a systematic analysis should be performed to determine which fluorescent tags maximize the CDK activity sensor's dynamic range.

When correlating DHB ratios to specific phases of the cell cycle, it is important to define interphase boundaries for any cell or tissue of interest. Our laboratory has observed significant differences in DHB ratios between tissues in *C. elegans*. For example, ventral uterine cells have higher DHB ratios in G1 compared with vulval precursor cells but lower DHB ratios in G2 [27]. To determine DHB ratios for G1, S, and G2, an S-phase reporter is required that can delineate the G1/S and S/G2 boundaries. However, an S-phase reporter is not necessary for assessing the proliferation-quiescence decision [23,27]. While drugs, genetic approaches, and fixation methods have been used to estimate DHB ratios for S-phase, these approaches do not provide the full range of DHB ratios for this phase. A fluorescently tagged PCNA reporter is the ideal tool for measuring the duration of S-phase. In S-phase, PCNA forms nuclear puncta at sites of DNA replication that can be readily detected by confocal microscopy. Recently, Zerjatke et al. [68] labeled endogenous PCNA with mRuby on its N-terminus. The authors described mRuby-PCNA as an all-in-one reporter of the cell cycle, but there is a caveat to consider. To decipher each phase of the cell cycle, investigators must follow the nuclear expression pattern of mRuby-PCNA over the length of a cell cycle. Otherwise, in the absence of PCNA puncta, it is difficult to distinguish G1 from G2 based on the nuclear expression of mRuby-PCNA alone. Nonetheless, PCNA is an established reporter of S-phase that can be used to calibrate the CDK activity sensor.

For the quantification of DHB ratios, histone H2B is often used as a nuclear marker to segment the nucleus and cytoplasm (Figure 1E). However, this approach occupies one of the fluorescent channels that could otherwise be used to visualize proteins of interest. An alternative approach to consider is the use of a nuclear envelope (NE) marker that strictly outlines the edge of the nucleus (Figure 1E). In theory, a NE marker tagged with the same fluorescent protein as the CDK activity sensor would open two or more fluorescent channels and facilitate the cytoplasmic-to-nuclear quantification of DHB by minimizing analysis to a single channel. To avoid interfering with the readout of the CDK activity sensor, the brightness and copy number of the fluorescent tag deserves careful consideration. Moreover, a NE marker accurately defines the outer boundary of the nucleus unlike histone H2B. This feature of NE markers could help reduce nuclear DHB signal from the cytoplasmic ring that is used to quantify cytoplasmic DHB [23]. As automated image segmentation methods improve (reviewed in [69]), this approach may overcome challenges associated with segmenting and tracking cells that are moving and dividing over time (Figure 1F).

Limitations

Beyond the restriction point and beginning in S-phase, $DHB_{994–1087}$ is phosphorylated by both CDK2 and CDK1 [33]. Therefore, the inability to uncouple CDK2 from CDK1 activity is a limitation of the CDK activity sensor. If measuring CDK1 activity is of importance, the CDK1 fluorescence resonance energy transfer (FRET) biosensor is an option. It was first developed in mammalian cells by Gavet and Pines [70], and it has since been applied in *Drosophila* embryos [71] and *Xenopus* egg extracts [72]. Another limitation of the CDK activity sensor is that it may become saturated in the presence of high CDK activity. A potential solution is the expression of multiple DHB fragments, with the caveat that they may abduct CDKs from their critical substrates. It is

also not possible to distinguish early, middle, and late CDK substrates when utilizing the CDK activity sensor, which may impact one's ability to determine cell-cycle order in plastic situations [73]. For example, during early embryonic development, the gap phases are omitted to accelerate the initial cell cycles [74–76]. The CDK activity sensor alone cannot detect this phenomenon or the future incorporation of gap phases. Despite these limitations, the sensor remains an attractive tool for monitoring the passage of cells through the cell cycle.

Concluding remarks

CDK activity sensors have emerged as powerful tools for studying the cell cycle in live cells. These biosensors have a streamlined and versatile design. Only a single fluorescently tagged substrate is required to track the cell cycle of an individual cell. These biosensors can be paired with any fluorescent reporter of the cell cycle or other proteins of interest. In the future, we envision researchers combining the CDK activity sensor with targeted protein degradation approaches, such as the auxin-inducible degron system [77–79], which could provide an outlet for conducting functional studies during the cell cycle [80]. These biosensors are also quantitative. Investigators can measure CDK activity in individual cells by quantifying the cytoplasmic-to-nuclear ratio of DHB using open-source software, such as ImageJ/FIJI [81]. Although quantification of DHB ratios by hand is a rate-limiting step, advances in automated image analysis, machine learning, and better image segmentation will facilitate high-throughput studies that examine the relationship between CDK activity and cell-cycle commitment in development and disease.

Perspectives

- CDK activity sensors are single-color, ratiometric biosensors for monitoring the cell cycle of individual cells.
- CDK activity sensors are highly adaptable and can be used in cell culture, orthotopic models, nematodes, fish, and flies.
- We anticipate that these biosensors will contribute to our understanding of cell-cycle control during cell invasion, migration, and growth in morphogenesis and cancer.

Competing Interests

D.Q.M. is a paid consultant for Arcadia Science.

Funding

M.A.Q.M. is supported by the National Cancer Institute (F30CA257383). D.Q.M. is supported by the National Institute of General Medical Sciences (R01GM121597) and the Damon Runyon Cancer Research Foundation (DRR-47-17).

Author Contributions

M.A.Q.M. and D.Q.M. defined an outline, M.A.Q.M. wrote a first draft, and M.A.Q.M. and D.Q.M. edited and revised the manuscript.

Acknowledgements

We thank Dr. Benjamin Martin and members of the Matus laboratory, including Taylor Medwig-Kinney and Frances Moore, for their comments and suggestions.

Abbreviations

CDK, cyclin-dependent kinase; DHB, DNA helicase B; FRET, fluorescence resonance energy transfer; FUCCI, fluorescent ubiquitination-based cell cycle indicator; H2B, histone 2B; KTR, kinase translocation reporter; NES, nuclear export signal; NLS, nuclear localization signal; PCNA, proliferating cell nuclear antigen; Rb, retinoblastoma.

Biochemical Society Transactions (2022) **50** 1081–1090
https://doi.org/10.1042/BST20211131

References

1 Howard, A. and Pelc, S.R. (1953) Synthesis of desoxyribonucleic acid in normal and irradiated cells and its relation to chromosome breakage. *Hered. Suppl.* **6**, 261–273
2 Pardee, A.B. (1974) A restriction point for control of normal animal cell proliferation. *Proc. Natl Acad. Sci. U.S.A.* **71**, 1286–1290 https://doi.org/10.1073/pnas.71.4.1286
3 Matthews, H.K., Bertoli, C. and de Bruin, R.A.M. (2022) Cell cycle control in cancer. *Nat. Rev. Mol. Cell Biol.* **23**, 74–88 https://doi.org/10.1038/s41580-021-00404-3
4 Sakaue-Sawano, A., Kurokawa, H., Morimura, T., Hanyu, A., Hama, H., Osawa, H. et al. (2008) Visualizing spatiotemporal dynamics of multicellular cell-cycle progression. *Cell* **132**, 487–498 https://doi.org/10.1016/j.cell.2007.12.033
5 Abe, T., Sakaue-Sawano, A., Kiyonari, H., Shioi, G., Inoue, K., Horiuchi, T. et al. (2013) Visualization of cell cycle in mouse embryos with Fucci2 reporter directed by *Rosa26* promoter. *Development* **140**, 237–246 https://doi.org/10.1242/dev.084111
6 Mort, R.L., Ford, M.J., Sakaue-Sawano, A., Lindstrom, N.O., Casadio, A., Douglas, A.T. et al. (2014) *Fucci2a:* A bicistronic cell cycle reporter that allows Cre mediated tissue specific expression in mice. *Cell Cycle* **13**, 2681–2696 https://doi.org/10.4161/15384101.2015.945381
7 Bajar, B.T., Lam, A.J., Badiee, R.K., Oh, Y.-H., Chu, J., Zhou, X.X. et al. (2016) Fluorescent indicators for simultaneous reporting of all four cell cycle phases. *Nat. Methods* **13**, 993–996 https://doi.org/10.1038/nmeth.4045
8 Grant, G.D., Kedziora, K.M., Limas, J.C., Cook, J.G. and Purvis, J.E. (2018) Accurate delineation of cell cycle phase transitions in living cells with PIP-FUCCI. *Cell Cycle* **17**, 2496–2516 https://doi.org/10.1080/15384101.2018.1547001
9 Oki, T., Nishimura, K., Kitaura, J., Togami, K., Maehara, A., Izawa, K. et al. (2015) A novel cell-cycle-indicator, mVenus-p27K–, identifies quiescent cells and visualizes G0–G1 transition. *Sci. Rep.* **4**, 4012 https://doi.org/10.1038/srep04012
10 Shirmanova, M.V., Gorbachev, D.A., Sarkisyan, K.S., Parnes, A.P., Gavrina, A.I., Polozova, A.V. et al. (2021) FUCCI-Red: a single-color cell cycle indicator for fluorescence lifetime imaging. *Cell. Mol. Life Sci.* **78**, 3467–3476 https://doi.org/10.1007/s00018-020-03712-7
11 Ando, R., Sakaue-Sawano, A., Shoda, K. and Miyawaki, A. (2020) Two new coral fluorescent proteins of distinct colors for sharp visualization of cell-cycle progression. *bioRxiv* https://doi.org/10.1101/2020.03.30.015156
12 Frei, M.S., Tarnawski, M., Roberti, M.J., Koch, B., Hiblot, J. and Johnsson, K. (2021) Engineered HaloTag variants for fluorescence lifetime multiplexing. *Nat. Methods* **19**, 65–70 https://doi.org/10.1038/s41592-021-01341-x
13 Capece, M., Tessari, A., Mills, J., Rampioni Vinciguerra, G.L., Lin, C., McElwain, B.K. et al. (2021) A novel auxin-inducible degron system for rapid, cell cycle-specific targeted proteolysis. *bioRxiv* https://doi.org/10.1101/2021.04.23.441203
14 Sugiyama, M., Sakaue-Sawano, A., Iimura, T., Fukami, K., Kitaguchi, T., Kawakami, K. et al. (2009) Illuminating cell-cycle progression in the developing zebrafish embryo. *Proc. Natl Acad. Sci. U.S.A.* **106**, 20812–20817 https://doi.org/10.1073/pnas.0906464106
15 Bouldin, C.M., Snelson, C.D., Farr, G.H. and Kimelman, D. (2014) Restricted expression of *cdc25a* in the tailbud is essential for formation of the zebrafish posterior body. *Genes Dev.* **28**, 384–395 https://doi.org/10.1101/gad.233577.113
16 Ogura, Y., Sakaue-Sawano, A., Nakagawa, M., Satoh, N., Miyawaki, A. and Sasakura, Y. (2011) Coordination of mitosis and morphogenesis: role of a prolonged G2 phase during chordate neurulation. *Development* **138**, 577–587 https://doi.org/10.1242/dev.053132
17 Zielke, N., Korzelius, J., van Straaten, M., Bender, K., Schuhknecht, G.F.P., Dutta, D. et al. (2014) Fly-FUCCI: a versatile tool for studying cell proliferation in complex tissues. *Cell Rep.* **7**, 588–598 https://doi.org/10.1016/j.celrep.2014.03.020
18 Özpolat, B.D., Handberg-Thorsager, M., Vervoort, M. and Balavoine, G. (2017) Cell lineage and cell cycling analyses of the 4d micromere using live imaging in the marine annelid *Platynereis dumerilii*. *eLife* **6**, e30463 https://doi.org/10.7554/eLife.30463
19 Dolfi, L., Ripa, R., Antebi, A., Valenzano, D.R. and Cellerino, A. (2019) Cell cycle dynamics during diapause entry and exit in an annual killifish revealed by FUCCI technology. *EvoDevo* **10**, 29 https://doi.org/10.1186/s13227-019-0142-5
20 Costa E, C., Otsuki, L., Rodrigo Albors, A., Tanaka, E.M. and Chara, O. (2021) Spatiotemporal control of cell cycle acceleration during axolotl spinal cord regeneration. *eLife* **10**, e55665 https://doi.org/10.7554/eLife.55665
21 Zielke, N. and Edgar, B.A. (2015) FUCCI sensors: powerful new tools for analysis of cell proliferation: FUCCI sensors. *Wiley Interdiscip. Rev. Dev. Biol.* **4**, 469–487 https://doi.org/10.1002/wdev.189
22 Luo, M., Li, J.-F., Yang, Q., Zhang, K., Wang, Z.-W., Zheng, S. et al. (2020) Stem cell quiescence and its clinical relevance. *World J. Stem Cells* **12**, 1307–1326 https://doi.org/10.4252/wjsc.v12.i11.1307
23 Spencer, S.L., Cappell, S.D., Tsai, F.-C., Overton, K.W., Wang, C.L. and Meyer, T. (2013) The proliferation-quiescence decision is controlled by a bifurcation in CDK2 activity at mitotic exit. *Cell* **155**, 369–383 https://doi.org/10.1016/j.cell.2013.08.062
24 Hahn, A.T., Jones, J.T. and Meyer, T. (2009) Quantitative analysis of cell cycle phase durations and PC12 differentiation using fluorescent biosensors. *Cell Cycle* **8**, 1044–1052 https://doi.org/10.4161/cc.8.7.8042
25 Gu, J., Xia, X., Yan, P., Liu, H., Podust, V.N., Reynolds, A.B. et al. (2004) Cell cycle-dependent regulation of a human DNA helicase that localizes in DNA damage foci. *Mol. Biol. Cell* **15**, 3320–3332 https://doi.org/10.1091/mbc.e04-03-0227
26 van Rijnberk, L.M., van der Horst, S.E.M., van den Heuvel, S. and Ruijtenberg, S. (2017) A dual transcriptional reporter and CDK-activity sensor marks cell cycle entry and progression in *C. elegans*. *PLoS ONE* **12**, e0171600 https://doi.org/10.1371/journal.pone.0171600
27 Adikes, R.C., Kohrman, A.Q., Martinez, M.A.Q., Palmisano, N.J., Smith, J.J., Medwig-Kinney, T.N. et al. (2020) Visualizing the metazoan proliferation-quiescence decision in vivo. *eLife* **9**, e63265 https://doi.org/10.7554/eLife.63265
28 Hur, W., Kemp, J.P., Tarzia, M., Deneke, V.E., Marzluff, W.F., Duronio, R.J. et al. (2020) CDK-regulated phase separation seeded by histone genes ensures precise growth and function of histone locus bodies. *Dev. Cell* **54**, 379–394.e6 https://doi.org/10.1016/j.devcel.2020.06.003
29 Meserve, J.H. and Duronio, R.J. (2021) Deciding when to exit. *eLife* **10**, e66591 https://doi.org/10.7554/eLife.66591
30 Morabito, R.D., Adikes, R.C., Matus, D.Q. and Martin, B.L. (2021) Cyclin-dependent kinase sensor transgenic zebrafish lines for improved cell cycle state visualization in live animals. *Zebrafish* **18**, 374–375 https://doi.org/10.1089/zeb.2021.0059
31 Leonhardt, H., Rahn, H.-P., Weinzierl, P., Sporbert, A., Cremer, T., Zink, D. et al. (2000) Dynamics of DNA replication factories in living cells. *J. Cell Biol.* **149**, 271–280 https://doi.org/10.1083/jcb.149.2.271
32 Brooks, R.F. (2021) Cell cycle commitment and the origins of cell cycle variability. *Front. Cell Dev. Biol.* **9**, 698066 https://doi.org/10.3389/fcell.2021.698066

33 Schwarz, C., Johnson, A., Kõivomägi, M., Zatulovskiy, E., Kravitz, C.J., Doncic, A. et al. (2018) A precise Cdk activity threshold determines passage through the restriction point. *Mol. Cell* **69**, 253–264.e5 https://doi.org/10.1016/j.molcel.2017.12.017
34 Zhao, M.L., Rabiee, A., Kovary, K.M., Bahrami-Nejad, Z., Taylor, B. and Teruel, M.N. (2020) Molecular competition in G1 controls when cells simultaneously commit to terminally differentiate and exit the cell cycle. *Cell Rep.* **31**, 107769 https://doi.org/10.1016/j.celrep.2020.107769
35 Miller, I., Min, M., Yang, C., Tian, C., Gookin, S., Carter, D. et al. (2018) Ki67 is a graded rather than a binary marker of proliferation versus quiescence. *Cell Rep.* **24**, 1105–1112.e5 https://doi.org/10.1016/j.celrep.2018.06.110
36 Barr, A.R., Cooper, S., Heldt, F.S., Butera, F., Stoy, H., Mansfeld, J. et al. (2017) DNA damage during S-phase mediates the proliferation-quiescence decision in the subsequent G1 via p21 expression. *Nat. Commun.* **8**, 14728 https://doi.org/10.1038/ncomms14728
37 Barr, A.R., Heldt, F.S., Zhang, T., Bakal, C. and Novák, B. (2016) A dynamical framework for the all-or-none G1/S transition. *Cell Syst.* **2**, 27–37 https://doi.org/10.1016/j.cels.2016.01.001
38 Gross, S.M., Mohammadi, F., Sanchez-Aguila, C., Zhan, P.J., Meyer, A.S. and Heiser, L.M. (2020) Analysis and modeling of cancer drug responses using cell cycle phase-specific rate effects. *bioRxiv* https://doi.org/10.1101/2020.07.24.219907
39 Nagasaka, K., Hossain, M.J., Roberti, M.J., Ellenberg, J. and Hirota, T. (2016) Sister chromatid resolution is an intrinsic part of chromosome organization in prophase. *Nat. Cell Biol.* **18**, 692–699 https://doi.org/10.1038/ncb3353
40 Chu, D., Nguyen, A., Smith, S.S., Vavrušová, Z. and Schneider, R.A. (2020) Stable integration of an optimized inducible promoter system enables spatiotemporal control of gene expression throughout avian development. *Biol. Open* **9**, bio.055343 https://doi.org/10.1242/bio.055343
41 Feringa, F.M., Krenning, L., Koch, A., van den Berg, J., van den Broek, B., Jalink, K. et al. (2016) Hypersensitivity to DNA damage in antephase as a safeguard for genome stability. *Nat. Commun.* **7**, 12618 https://doi.org/10.1038/ncomms12618
42 Wutz, G., Várnai, C., Nagasaka, K., Cisneros, D.A., Stocsits, R.R., Tang, W. et al. (2017) Topologically associating domains and chromatin loops depend on cohesin and are regulated by CTCF, WAPL, and PDS5 proteins. *EMBO J.* **36**, 3573–3599 https://doi.org/10.15252/embj.201798004
43 Gross, S.M. and Rotwein, P. (2016) Unraveling growth factor signaling and cell cycle progression in individual fibroblasts. *J. Biol. Chem.* **291**, 14628–14638 https://doi.org/10.1074/jbc.M116.734194
44 Di Martino, J.S., Nobre, A.R., Mondal, C., Taha, I., Farias, E.F., Fertig, E.J. et al. (2022) A tumor-derived type III collagen-rich ECM niche regulates tumor cell dormancy. *Nat. Cancer* **3**, 90–107 https://doi.org/10.1038/s43018-021-00291-9
45 Yoon, K.-J., Ringeling, F.R., Vissers, C., Jacob, F., Pokrass, M., Jimenez-Cyrus, D. et al. (2017) Temporal control of mammalian cortical neurogenesis by m^6A methylation. *Cell* **171**, 877–889.e17 https://doi.org/10.1016/j.cell.2017.09.003
46 Yang, H.W., Cappell, S.D., Jaimovich, A., Liu, C., Chung, M., Daigh, L.H. et al. (2020) Stress-mediated exit to quiescence restricted by increasing persistence in CDK4/6 activation. *eLife* **9**, e44571 https://doi.org/10.7554/eLife.44571
47 Regot, S., Hughey, J.J., Bajar, B.T., Carrasco, S. and Covert, M.W. (2014) High-sensitivity measurements of multiple kinase activities in live single cells. *Cell* **157**, 1724–1734 https://doi.org/10.1016/j.cell.2014.04.039
48 Dwivedi, V.K., Pardo-Pastor, C., Droste, R., Kong, J.N., Tucker, N., Denning, D.P. et al. (2021) Replication stress promotes cell elimination by extrusion. *Nature* **593**, 591–596 https://doi.org/10.1038/s41586-021-03526-y
49 Deng, T., Stempor, P., Appert, A., Daube, M., Ahringer, J., Hajnal, A. et al. (2020) The *Caenorhabditis elegans* homolog of the Evi1 proto-oncogene, *egl-43*, coordinates G1 cell cycle arrest with pro-invasive gene expression during anchor cell invasion. *PLoS Genet.* **16**, e1008470 https://doi.org/10.1371/journal.pgen.1008470
50 Matus, D.Q., Lohmer, L.L., Kelley, L.C., Schindler, A.J., Kohrman, A.Q., Barkoulas, M. et al. (2015) Invasive cell fate requires G1 cell-cycle arrest and histone deacetylase-mediated changes in gene expression. *Dev. Cell* **35**, 162–174 https://doi.org/10.1016/j.devcel.2015.10.002
51 Smith, J.J., Xiao, Y., Parsan, N., Medwig-Kinney, T.N., Martinez, M.A.Q., Moore, F.E.Q. et al. (2022) The SWI/SNF chromatin remodeling assemblies BAF and PBAF differentially regulate cell cycle exit and cellular invasion *in vivo*. *PLoS Genet.* **18**, e1009981 https://doi.org/10.1371/journal.pgen.1009981
52 Ahier, A. and Jarriault, S. (2014) Simultaneous expression of multiple proteins under a single promoter in *Caenorhabditis elegans* via a versatile 2A-based toolkit. *Genetics* **196**, 605–613 https://doi.org/10.1534/genetics.113.160846
53 Brauchle, M., Baumer, K. and Gönczy, P. (2003) Differential activation of the DNA replication checkpoint contributes to asynchrony of cell division in *C. elegans* embryos. *Curr. Biol.* **13**, 819–827 https://doi.org/10.1016/S0960-9822(03)00295-1
54 Furuta, T. and Arur, S. (2018) GFP::PCN-1 does not reliably mark S phase in *C. elegans* adult germline progenitor zone cells. *MicroPubl. Biol.* **2018**, 10.17912/W20W9G https://doi.org/10.17912/W20W9G
55 Sternberg, P.W. and Horvitz, H.R. (1986) Pattern formation during vulva development in *C. elegans*. *Cell* **44**, 761–772 https://doi.org/10.1016/0092-8674(86)90842-1
56 van der Horst, S.E.M., Cravo, J., Woollard, A., Teapal, J. and van den Heuvel, S. (2019) *C. elegans* Runx/CBFβ suppresses POP-1 TCF to convert asymmetric to proliferative division of stem cell-like seam cells. *Development* **146**, dev180034 https://doi.org/10.1242/dev.180034
57 Provost, E., Rhee, J. and Leach, S.D. (2007) Viral 2A peptides allow expression of multiple proteins from a single ORF in transgenic zebrafish embryos. *Genesis* **45**, 625–629 https://doi.org/10.1002/dvg.20338
58 Strzyz, P.J., Lee, H.O., Sidhaye, J., Weber, I.P., Leung, L.C. and Norden, C. (2015) Interkinetic nuclear migration is centrosome independent and ensures apical cell division to maintain tissue integrity. *Dev. Cell* **32**, 203–219 https://doi.org/10.1016/j.devcel.2014.12.001
59 Leung, L., Klopper, A.V., Grill, S.W., Harris, W.A. and Norden, C. (2012) Apical migration of nuclei during G2 is a prerequisite for all nuclear motion in zebrafish neuroepithelia. *Development* **139**, 2635–2635 https://doi.org/10.1242/dev.085456
60 Liu, C., Konagaya, Y., Chung, M., Daigh, L.H., Fan, Y., Yang, H.W. et al. (2020) Altered G1 signaling order and commitment point in cells proliferating without CDK4/6 activity. *Nat. Commun.* **11**, 5305 https://doi.org/10.1038/s41467-020-18966-9
61 Duronio, R.J. and Marzluff, W.F. (2017) Coordinating cell cycle-regulated histone gene expression through assembly and function of the histone locus body. *RNA Biol.* **14**, 726–738 https://doi.org/10.1080/15476286.2016.1265198
62 Hazeslip, L., Zafar, M.K., Chauhan, M.Z. and Byrd, A.K. (2020) Genome maintenance by DNA helicase B. *Genes* **11**, 578 https://doi.org/10.3390/genes11050578
63 Alliance of Genome Resources Consortium, Agapite, J., Albou, L.-P., Aleksander, S.A., Alexander, M., Anagnostopoulos, A.V. et al. (2022) Harmonizing model organism data in the alliance of genome resources. *Genetics* **220**, iyac022 https://doi.org/10.1093/genetics/iyac022

Biochemical Society Transactions (2022) **50** 1081–1090
https://doi.org/10.1042/BST20211131

64 Cranfill, P.J., Sell, B.R., Baird, M.A., Allen, J.R., Lavagnino, Z., de Gruiter, H.M. et al. (2016) Quantitative assessment of fluorescent proteins. *Nat. Methods* **13**, 557–562 https://doi.org/10.1038/nmeth.3891
65 Heppert, J.K., Dickinson, D.J., Pani, A.M., Higgins, C.D., Steward, A., Ahringer, J. et al. (2016) Comparative assessment of fluorescent proteins for in vivo imaging in an animal model system. *Mol. Biol. Cell* **27**, 3385–3394 https://doi.org/10.1091/mbc.e16-01-0063
66 Lambert, T.J. (2019) FPbase: a community-editable fluorescent protein database. *Nat. Methods* **16**, 277–278 https://doi.org/10.1038/s41592-019-0352-8
67 Shemiakina, I.I., Ermakova, G.V., Cranfill, P.J., Baird, M.A., Evans, R.A., Souslova, E.A. et al. (2012) A monomeric red fluorescent protein with low cytotoxicity. *Nat. Commun.* **3**, 1204 https://doi.org/10.1038/ncomms2208
68 Zerjatke, T., Gak, I.A., Kirova, D., Fuhrmann, M., Daniel, K., Gonciarz, M. et al. (2017) Quantitative cell cycle analysis based on an endogenous all-in-one reporter for cell tracking and classification. *Cell Rep.* **19**, 1953–1966 https://doi.org/10.1016/j.celrep.2017.05.022
69 Kohrman, A.Q., Kim-Yip, R.P. and Posfai, E. (2021) Imaging developmental cell cycles. *Biophys. J.* **120**, 4149–4161 https://doi.org/10.1016/j.bpj.2021.04.035
70 Gavet, O. and Pines, J. (2010) Progressive activation of CyclinB1-Cdk1 coordinates entry to mitosis. *Dev. Cell* **18**, 533–543 https://doi.org/10.1016/j.devcel.2010.02.013
71 Deneke, V.E., Melbinger, A., Vergassola, M. and Di Talia, S. (2016) Waves of Cdk1 activity in S phase synchronize the cell cycle in *Drosophila* embryos. *Dev. Cell* **38**, 399–412 https://doi.org/10.1016/j.devcel.2016.07.023
72 Maryu, G. and Yang, Q. (2021) Nuclear-cytoplasmic compartmentalization promotes robust timing of mitotic events by cyclin B1-Cdk1. *bioRxiv* https://doi.org/10.1101/2021.07.28.454130
73 Swaffer, M.P., Jones, A.W., Flynn, H.R., Snijders, A.P. and Nurse, P. (2016) CDK substrate phosphorylation and ordering the cell cycle. *Cell* **167**, 1750–1761.e16 https://doi.org/10.1016/j.cell.2016.11.034
74 Kipreos, E.T. and van den Heuvel, S. (2019) Developmental control of the cell cycle: insights from *Caenorhabditis elegans*. *Genetics* **211**, 797–829 https://doi.org/10.1534/genetics.118.301643
75 Ferree, P.L., Deneke, V.E. and Di Talia, S. (2016) Measuring time during early embryonic development. *Semin. Cell Dev. Biol.* **55**, 80–88 https://doi.org/10.1016/j.semcdb.2016.03.013
76 Płusa, B. and Piliszek, A. (2020) Common principles of early mammalian embryo self-organisation. *Development* **147**, dev183079 https://doi.org/10.1242/dev.183079
77 Negishi, T., Kitagawa, S., Horii, N., Tanaka, Y., Haruta, N., Sugimoto, A. et al. (2021) The auxin-inducible degron 2 (AID2) system enables controlled protein knockdown during embryogenesis and development in *Caenorhabditis elegans*. *Genetics* **220**, iyab218 https://doi.org/10.1093/genetics/iyab218
78 Hills-Muckey, K., Martinez, M.A.Q., Stec, N., Hebbar, S., Saldanha, J., Medwig-Kinney, T.N. et al. (2021) An engineered, orthogonal auxin analog/AtTIR1(F79G) pairing improves both specificity and efficacy of the auxin degradation system in *Caenorhabditis elegans*. *Genetics* **220**, iyab174 https://doi.org/10.1093/genetics/iyab174
79 Yesbolatova, A., Saito, Y., Kitamoto, N., Makino-Itou, H., Ajima, R., Nakano, R. et al. (2020) The auxin-inducible degron 2 technology provides sharp degradation control in yeast, mammalian cells, and mice. *Nat. Commun.* **11**, 5701 https://doi.org/10.1038/s41467-020-19532-z
80 Suski, J.M., Ratnayeke, N., Braun, M., Zhang, T., Strmiska, V., Michowski, W. et al. (2022) CDC7-independent g1/S transition revealed by targeted protein degradation. *Nature* **605**, 357–365 https://doi.org/10.1038/s41586-022-04698-x
81 Schneider, C.A., Rasband, W.S. and Eliceiri, K.W. (2012) NIH image to ImageJ: 25 years of image analysis. *Nat. Methods* **9**, 671–675 https://doi.org/10.1038/nmeth.2089